RESEARCH ARTICLE OPEN ACCESS

Endoluminal Biopsy for Molecular Profiling of Human Brain Vascular Malformations

Ethan Winkler, MD, PhD, David Wu, BS, Eugene Gil, BS, David McCoy, MS, Kazim Narsinh, MD, Zhengda Sun, PhD, Kerstin Mueller, PhD, Jayden Ross, BA, Helen Kim, PhD, Shantel Weinsheimer, PhD, Mitchel Berger, MD, Tomasz Nowakowski, PhD, Daniel Lim, MD, PhD, Adib Abla, MD,* and Daniel Cooke, MD*

Correspondence
Dr. Cooke
daniel.cooke@ucsf.edu, or Dr. Abla
adib.abla@ucsf.edu

Neurology® 2022;98:e1637-e1647. doi:10.1212/WNL.0000000000200109

MORE ONLINE

Videos

Abstract

Background and Objectives

Ras–mitogen-activated protein kinase (MAPK) signaling abnormalities occur in most brain arteriovenous malformations (bAVMs). No means exist to molecularly profile bAVMs without open surgery, limiting precision medicine approaches to treatment. Here, we report use of endoluminal biopsy of the vessel lumen of bAVMs to characterize gene expression and blood flow–mediated transcriptional changes in living patients.

Methods

Endoluminal biopsy and computational fluid dynamic modeling (CFD) were performed in adults with unruptured AVMs with cerebral angiography. Each patient underwent surgical resection and cell sampling from a contiguous arterial segment. Fluorescence-assisted cell sorting enriched endothelial cells, which were sequenced on an Illumina HiSeq 4000 sequencer. Gene expression was quantified with RNA sequencing (RNAseq). Differential gene expression, ontology, and correlative analyses were performed. Results were validated with quantitative reverse transcription PCR (RT-qPCR).

Results

Endoluminal biopsy was successful in 4 patients without complication. Endoluminal biopsy yielded 269.0 ± 79.9 cells per biopsy (control 309.2 ± 86.6 cells, bAVM 228.8 ± 133.4 cells). RNAseq identified 106 differentially expressed genes (DEGs) in bAVMs (false discovery rate ≤0.05). DEGs were enriched for bAVM pathogenic cascades, including Ras-MAPK signaling ($p < 0.05$), and confirmed with RT-qPCR and a panel predictive of MAPK/extracellular signal-regulated kinase inhibitor response. Compared to patient-matched surgically excised tissues, endoluminal biopsy detected 83.3% of genes, and genome-wide expression strongly correlated (Pearson $r = 0.77$). Wall shear stress measured by CFD correlated with inflammatory pathway upregulation. Comparison of pre-embolization and postembolization samples confirmed flow-mediated gene expression changes.

Discussion

Endoluminal biopsy allows molecular profiling of bAVMs in living patients. Gene expression profiles are similar to those of tissues acquired with open surgery and identify potentially targetable Ras-MAPK signaling abnormalities in bAVMs. Integration with CFD allows determination of flow-mediated transcriptomic alterations. Endoluminal biopsy may help facilitate trials of precision medicine approaches to bAVMs in humans.

*These authors contributed equally and are co-corresponding authors.

From the Department of Neurological Surgery (E.W., D.W., E.G., J.R., M.B., D.L., A.A.), Department of Radiology and Biomedical Imaging (D.M., K.N., Z.S., D.C.), Center for Cerebrovascular Research (H.K., S.W.), Department of Psychiatry (T.N.), Department of Behavioral Sciences (T.N.), and Eli and Edythe Broad Center for Regeneration Medicine and Stem Cell Research (T.N., D.L.), University of California San Francisco; Siemens Medical Solutions Inc (K.M.), Malvern, PA; and Department of Anatomy (J.R., T.N.), University of California San Francisco, Chan Zuckerberg Biohub.

Go to Neurology.org/N for full disclosures. Funding information and disclosures deemed relevant by the authors, if any, are provided at the end of the article.

The Article Processing Charge was funded by the authors.

Glossary

AVM = arteriovenous malformation; **bAVM** = brain AVM; **CBF** = cerebral blood flow; **CFD** = computational fluid dynamic; **DEG** = differentially expressed gene; **DSA** = digital subtraction angiography; **FACS** = fluorescence-activated cell sorting; **FDR** = false discovery rate; **MAPK** = mitogen-activated protein kinase; **MEK** = MAPK/extracellular signal-regulated kinase; **qPCR** = quantitative PCR; **RNAseq** = RNA sequencing; **scRNAseq** = single-cell RNAseq; **TAWSS** = time-averaged wall shear stress; **3D** = 3-dimensional.

One type of brain vascular malformation known as arteriovenous malformation (AVM) is a tangle of blood vessels that form direct connections between arteries and veins.[1] A subset of brain AVMs (bAVMs) result in intracerebral hemorrhage and are a leading cause of brain hemorrhage in young people.[2] However, the majority of bAVMs do not hemorrhage. Randomized controlled trials have suggested that interventional therapy such as endovascular embolization, stereotactic radiosurgery, or surgical resection is associated with higher rates of death and stroke than observation, and treatment remains controversial.[3]

Precision medicine approaches have revolutionized clinical care, most notably in oncology. Most AVMs (>95%) were thought to arise without clear genetic cause,[4] but renewed sequencing efforts have recently identified somatic activating variants within the Ras–mitogen-activated protein kinase (MAPK) signaling pathway such as the proto-oncogenes *KRAS* and *BRAF* in a majority of sporadic bAVMs.[5,6] Targeted inhibition of Ras-MAPK pathways reverses bAVM pathology in experimental models and is being trialed in extracranial vascular malformations.[6,7] Despite the ability to identify therapeutic targets, stereotactic brain biopsy techniques are not safe for many cerebrovascular pathologies due to risk of brain hemorrhage. Therefore, molecular profiling is performed only on vascular malformations removed with open surgery. This has several consequences: (1) the information obtained has little influence on clinical decision-making; (2) precision medicine treatment guided by the molecular profile of bAMVs is not possible; and (3) no molecular information is available from vascular malformations that are not surgically resected. As a result, there is presently no means to extract molecular information from human cerebrovascular pathologies in living patients.

To address this barrier to translation of cerebrovascular precision medicine in humans, we sought to use cerebral angiography, the diagnostic gold standard, to sample cells of the vessel lumen from within the cerebrovasculature. Here, we report our case series demonstrating feasibility and accuracy of cerebral angiography–guided endoluminal biopsy to molecularly profile bAVMs with next-generation RNA sequencing (RNAseq), to identify therapeutically targetable pathways, and to deduce flow-mediated transcriptomic alterations from unruptured bAVMs in living patients.

Methods

Standard Protocol Approvals, Registrations, and Patient Consents

Human bAVM samples and clinical data were obtained from the University of California San Francisco with protocols approved for human experimentation from the institutional review board and ethics committee (Institutional Review Board No. 15-16403). In addition to the standard surgical consent, written informed consent was obtained, permitting collection of an additional coil during treatment for the specific purpose of research. As part of the institutional review board, formal stopping rules were in place such as a single procedural hemorrhagic or ischemic stroke.

Patients were screened from outpatient clinics and in-hospital census lists. For this initial experience, only adults (>18 years of age) with unruptured AVMs undergoing flow-reductive embolization for subsequent microsurgical resection of the AVM were included. Exclusion criteria included AVMs that had previously or currently ruptured; the presence of high-risk features, e.g., flow-related aneurysms, or cerebrovascular anatomy not conducive to catheterization, e.g., vascular tortuosity or unfavorable aortic arch anatomy; or AVMs that were not to be treated with surgical resection. Clinical data are summarized in Table 1.

Endovascular Biopsy

Digital subtraction angiography (DSA) was performed in standard fashion on either an Artis Q or Artis Zee biplane angiographic system (Siemens Healthineers AG, Forchheim, Germany). Endovascular biopsy was performed as we have previously described.[8,9] All patients were administered general anesthesia, and transfemoral access was obtained under ultrasound guidance. After control femoral angiogram, a 0.035-in Benson or J-curved guide wire was placed through the sheath to contact with the endothelial lining of the iliac artery and kept in this location for ≈1 minute. The wire was removed, and the distal 3 cm was cut and placed in a 3-mL LoBind Eppendorf microcentrifuge tube containing chilled cell dissociation buffer (Thermo Fischer Scientific, Waltham, MA). A postsampling femoral angiogram was then performed to exclude any procedure-associated arterial dissection. This sample served as a patient-matched control from an uninvolved, systemic artery.

All patients then received an IV bolus of heparin to ensure an activated clotting time that was 2 times baseline or >250

Table 1 Patient Demographics and Cellular Yield With Endoluminal Sampling of Brain AVMs

				Endoluminal cell yield, n cells		Surgical cell yield, n cells	
Age, y	Sex	Location	SM grade	Iliac artery	AVM	AVM artery	AVM nidus
31	F	Parieto-occipital	1	140	14	1,052	9,726
49	M	Parieto-occipital	1	528	57	828	2,782
48	M	Temporal	4	206	244	157	282
23	F	Occipital	2	363	600	NC	NC
			Mean	309.2 ± 86.6	228.8 ± 133.4	679.0 ± 268.9	4,263.3 ± 2,825.1

Abbreviations: AVM = arteriovenous malformation; NC = not collected; SM = Spetzler-Martin.

seconds; this is standard practice to reduce thromboembolic complications with cerebral angiography. A diagnostic cerebral angiogram was then performed with telescoping guide and microcatheters tailored to each patient's cerebrovascular anatomy. Three-dimensional (3D) rotation angiography was performed with a Mark7 power injector (MedRad, Beek, the Netherlands) to inject the primary arterial supply of the AVM and to completely characterize the 3D anatomy of the AVM. A short arterial segment of 1 of the feeding arterial pedicles was identified a priori as the intended site of the endovascular biopsy. Site selection depended on several selection criteria: (1) the artery was intended to be subsequently embolized for the purposes of reducing flow for surgery the following day; (2) the artery could be safely accessed with a microcatheter; and (3) the arterial segment was juxtaposed to the AVM nidus (a distance <≈1 cm). The nidus was not sampled endovascularly due to heightened procedural risk.

After identification of the biopsy site, superselective microcatheterization of the desired arterial segment was performed under fluoroscopic guidance. Microcatheter position was confirmed with a focused angiogram. A platinum detachable coil was matched to the size of the parent vessel and deployed through the microcatheter, contacting the vessel lumen only at the desired biopsy site. After 1 minute of luminal contact, the coil was resheathed and removed from the telescoping catheters that protected it from contacting other vessel segments. The removed coil was then cut and placed into a 3-mL LoBind Eppendorf microcentrifuge tube containing chilled cell dissociation buffer. New coils were selected, and coil embolization was carried out per routine practice to reduce blood flow to the AVM for open neurosurgical resection. Procedural steps of the endovascular biopsy are shown in Video 1.

Computational Fluid Dynamic Modeling

A computational fluid dynamic (CFD) approach was used to compute the velocity field through the vasculature of interest and through the cardiac cycle. CFD simulations require accurate specification of boundary conditions, namely the luminal surface geometry and the inlet flow waveform through the cardiac cycle. The luminal contours were extracted with a level-set representation of the complex surface from the 3D DSA images acquired on either an Artis Q or Artis Zee biplane angiographic system (Siemens Healthineers AG). Images were transferred to a clinical postprocessing workstation and reconstructed on a 512 × 512 matrix with a smooth HU kernel, resulting in ≈0.8-mm actual resolution. The resulting reconstructed 3D DSA volumes were exported and loaded onto a research workstation with the available CFD modeling research prototype (Siemens Healthineers AG). Before processing, the site of endoluminal biopsy was marked in the 3D volume in order to perform CFD analysis on the same vessel segment close to the nidus.[10]

The prototype CFD solver (Siemens Healthineers AG) uses a GPU-optimized Lattice-Boltzmann method with a multi-relaxation time approximation.[11,12] In this approach, the incompressible Navier-Stokes equations are solved according to the finite volume method, and the pulsatile velocity field (3D + t, i.e., in space and through the cardiac cycle) is computed on a cartesian grid at 0.2-mm isotropic spatial resolution. This allows the determination of secondary hemodynamic descriptors such as the wall shear stress. The velocity waveform was adapted from the inflow velocity profile as previously described, which is based on 2-dimensional phase-contrast MRI measurements.[13,14] To ensure convergence, flow computations were performed over 2 heartbeats with a time step of 5×10^{-4} seconds, and results were output every 0.05 seconds. At all outflow boundaries, the pressure was fixed to 0 Pa. The blood density and viscosity were assumed to be 0.001 g/mm^3 and 0.004 Pa·s, respectively.

Open Neurosurgical Sampling

Patients were observed overnight in the intensive care unit and were taken to the neurosurgical operative suite the following day. All patients were placed under general anesthesia. A craniotomy was tailored to each patient with neuronavigational software in standard fashion, and microsurgical resection was performed with aide of a Zeiss OPMI Pentero 800 operative microscope (Carl Zeiss AG, Oberkochen, Germany). Direct microscopic visualization, including intraoperative indocyanine green angiography,[15] and confirmation with neuronavigational software (BrainLab, Munich,

Germany) identified feeding arteries and the nidus and draining veins of the AVM. To maintain 3D orientation, aneurysm clips and AVM microclips (Aesculap, Inc, Center Valley, PA) of different sizes were placed under direct visualization onto feeding arteries of interest, including the endovascular biopsy site, and to mark the AVM nidus. After AVM removal, the AVM was microdissected into the arterial segment from the biopsy site and nidus, and tissue samples from each site were placed in preoxygenated chilled Dulbecco modified Eagle medium (Thermo Fisher Scientific) and transported to the laboratory for subsequent dissociation.

Cell Preparation and Fluorescence-Activated Cell Sorting

For cell samples from endovascular biopsy, samples were vortexed for 30 seconds in cell dissociation buffer to liberate cells, and the cut wire or coil was discarded. Cells were subsequently spun down, and erythrocytes were lysed with incubation in ACK lysing buffer (Thermo Fisher Scientific). Cells were washed with phosphate-buffered saline. All tissues from open surgical resection were microdissected with a No. 15 scalpel into ≈1 × 1–mm cubes and subsequently dissociated with 0.2% collagenase type 2 (Worthington Biochemical corporation, Lakewood, NJ). Erythrocytes were lysed with incubation in ACK lysing buffer, and cell suspension was filtered through a sterile 40-μm filter to remove debris and washed with phosphate-buffered saline.

Cell suspensions were resuspended in fluorescence-activated cell sorting (FACS) buffer and stained with a modified protocol as we described.[8,9,16] Cells were stained with Alexa Fluor 647–conjugated monoclonal anti-human CD31 antibody (BD Biosciences, San Jose, CA) and 4′,6-diamidino-2-phenylindole (DAPI, Thermo Fisher Scientific). Cells were subsequently fluorescently sorted on a BD FACSAria II Flow Cytometer (BD Biosciences). Nonviable cells were excluded on the basis of DAPI positivity, and endothelial enrichment was performed through positive selection of CD31 cells. Viable cells enriched for endothelium were therefore considered to be CD31-positive, DAPI-negative cells.

Library Preparation and Bulk RNAseq

Library preparation and sequencing of samples were performed by investigators blinded to pathology. cDNA sequencing libraries were created directly with application of the SEQuoia complete RNA library prep kit (Biorad Laboratories, Inc, Hercules, CA) to whole cells as described by the manufacturer. rRNA was depleted with proprietary technology postlibrary generation (Biorad Laboratories, Inc). All of the final libraries underwent quality control analysis with the Agilent D1000 ScreenTape System (Agilent Technologies, Santa Clara, CA) and were sequenced on an Illumina HiSeq 4000, single-end 50 base pair reads, multiplexed at 6 samples per lane.

Quantitative PCR

To confirm RNAseq results, quantitative PCR (qPCR) was performed on generated cDNA. A subset of 5 differentially expressed genes (DEGs) identified with highest score determined by $-\log_{10}$ p-value × abs(β) and a bioinformatic panel sensitive to activation of MAPK signaling and predictive of response of MAPK/extracellular signal-regulated kinase (MEK) inhibitors were used for this analysis.[17] Primers were designed with the use of Fluidigm D3 assay design software[18] (Fluidigm Corp, South San Francisco, CA), and assay identifications are given in eTable 1, links.lww.com/WNL/B817. qPCR was performed with SBYR green (Roche Applied Science, Penzberg, Germany) on a LightCycler 480 II (Roche Applied Science). Relative gene expression was calculated with the delta-delta C_T method using β-actin (*ACTB*) as a housekeeping gene. Data are presented as mean ± SD for 4 biological replicates.

Single-Cell RNAseq

To confirm endothelial enrichment via FACS, we sorted individual CD31-positive, DAPI-negative cells acquired via endoluminal biopsy and prepared single-cell RNAseq (scRNAseq) libraries using the Smart-seq2 protocol on 96-sorted cells as previously described.[19] Final libraries underwent quality control analysis with the Agilent D1000 ScreenTape System (Agilent Technologies) and were sequenced on an Illumina HiSeq 4000 with paired-end 100 base pair reads.

Data Analyses

For sequencing data, sequencing quality was confirmed with FastQC, and adaptors were trimmed with Cutadapt. Reads were pseudoaligned to ENSEMBL GRCh38 transcriptome using Kallisto with 100 bootstrap samples.[20] For scRNAseq data, gene count matrices were generated and analyzed with Seurat.[21] Detected genes were defined as those with a transcript per million. Gene-level differential gene expression analysis was performed with Sleuth, and β serves as an estimate of the fold change as previously reported.[22] Genes with a false discovery rate (FDR)–adjusted value of $q < 0.05$ were considered to be differentially expressed. Gene ontology analyses were performed on DEGs with an FDR-adjusted value of $q < 0.1$ with EnrichR.[23] For in vivo flow modeling, Pearson correlation coefficients were used to deduce the relationship of time-averaged wall shear stress (TAWSS) with gene expression (expressed as transcripts per million) for each transcript across individuals. Genes with a correlation coefficient ≥0.6 or ≤−0.6 were defined to be correlated genes. All data analyses and visualizations were performed with R version 3.6.3 (R Foundation for Statistical Computing, Vienna, Austria).

Data Availability

Anonymized data not published within this article will be made available by request from any qualified investigator.

Results

Endoluminal Biopsy Detects Pathogenic and Targetable Molecular Changes in bAVMs

Endoluminal biopsy was performed in all patients without complication (Figure 1A). Patient demographic information is summarized in Table 1. On average, 269.0 ± 79.9 CD31-positive, DAPI-negative viable cells were recovered per site

(control 309.2 ± 86.6 cells, AVM 228.8 ± 133.4 cells) (Table 1). With the FACS gating parameters used, scRNAseq confirmed enrichment of endothelial cells that make up 71.9% of cells sampled on the basis of canonical marker expression (eFigure 1A, links.lww.com/WNL/B817). RNAseq profiling of endoluminal biopsied cells identified 106 DEGs (FDR <0.05) (Figure 1B and eTable 2, links.lww.com/WNL/B817). Pathway analysis showed that DEGs were enriched for bAVM pathogenic pathways such as MAPK signaling,[5,6] angiogenesis (Rho-mediated cell motility, serum response factor activation, thrombin signaling),[24,25] and inflammation (antigen processing) (Figure 1C).[26] Ontologic molecular function analysis confirmed enrichment of serine/threonine and protein kinase activity and binding to the small GTPases Ras and Rab (Figure 1C).

To confirm these findings, we next performed reverse transcription qPCR analysis to verify DEGs and MAPK activation.

Figure 1 Endoluminal Biopsy Detects Pathologic Gene Expression Changes in Brain AVMs

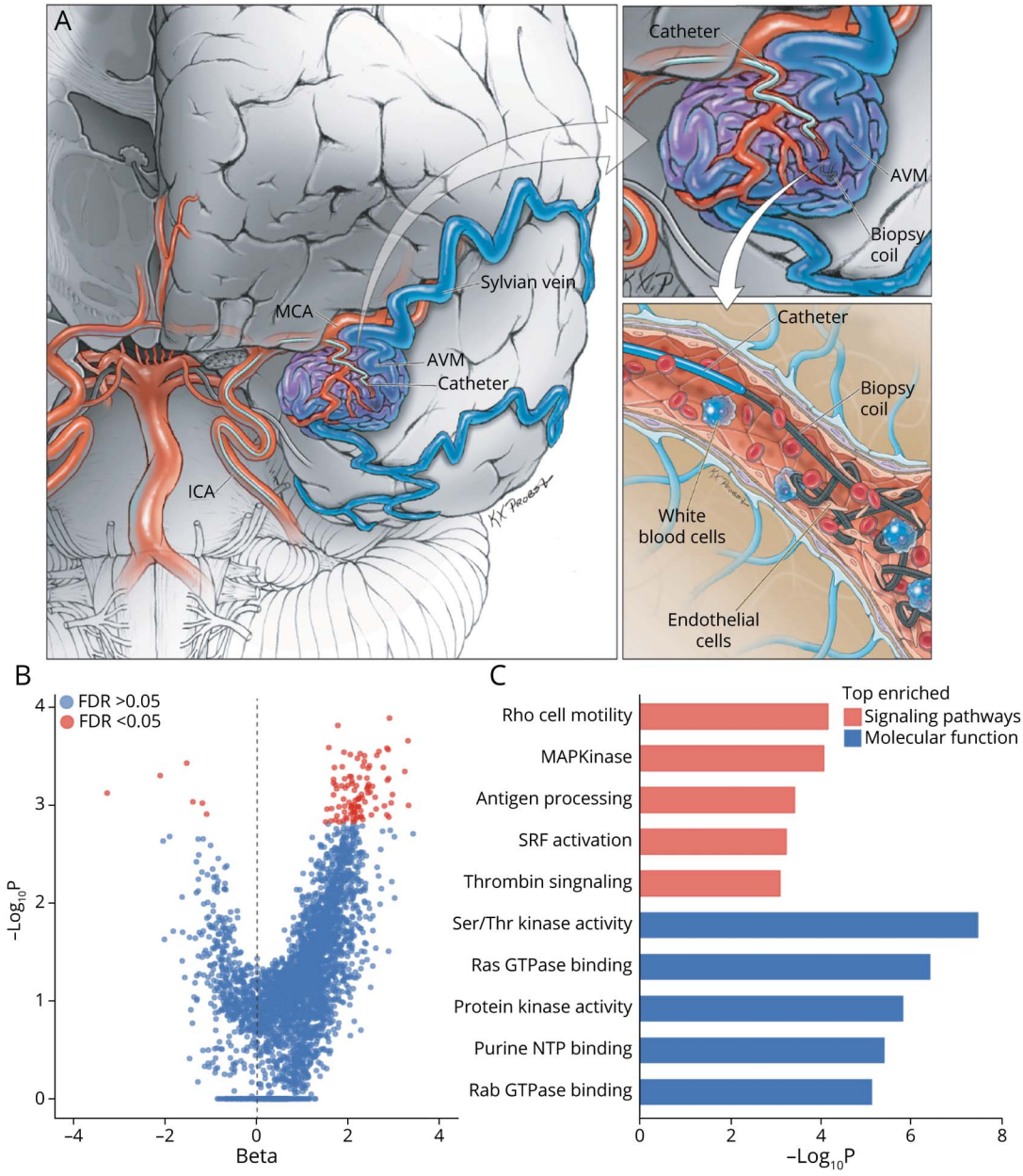

(A) Endoluminal biopsy is achieved through image-guided placement of a cerebral angiography microcatheter into the lumen of an arteriovenous malformation (AVM). A platinum coil is then deployed, contacting and removing the cellular lining of the artery. The coil is removed, and subsequent fluorescence-activated cell sorting enriches for endothelium. Figure courtesy of Kenneth Xavier Probst. (B) Volcano plot of RNA sequencing gene expression from AVM and patient-matched uninvolved vessel. Beta is the effect size. (C) Bar graph showing ontologic analysis of differentially expressed genes. Orange indicates signaling pathways; blue, molecular function. FDR =false discovery rate; ICA = internal carotid artery; MAPkinase = mitogen-activated protein kinase; MCA = middle cerebral artery; NTP = nucleoside triphosphate; SRF = serum response factor.

We confirmed the differential expression of 5 genes (*NBPF19*, *IFITM1*, *FBLX18*, *TNFRSR10C*, and *MARCHF8*) among the 10 most DEGs (Figure 2A). We investigated MAPK activation with a gene panel independently shown to also predict response to MEK inhibitors in human cancer.[17] This analysis demonstrated statistically significant upregulation of 7 of 10 genes supporting MAPK activation (Figure 2B). Thus, endoluminal biopsy recovers primary cells that reflect molecular events in the malformed vasculature, enables direct molecular profiling, and identifies potential therapeutic targets without the need for surgery.

Endoluminal Biopsy Closely Approximates Gene Expression Profiling From Surgically Excised AVMs

We next sought to compare gene expression profiles obtained from endoluminally biopsied cells with surgically acquired tissues from the same patients, an important technical validation benchmark. We optimized a microsurgical technique to preserve 3D orientation of the bAVM and to ensure sampling from an arterial segment contiguous with the biopsy site (Figure 3A). RNAseq analysis demonstrates that endoluminal biopsy detects the vast majority (83.3%) of the genes identified in surgical tissue (Figure 3B). Gene expression profiles from endoluminal and surgically acquired cells correlated well genome-wide (Pearson r = 0.77, Figure 3C), supporting good concordance between techniques. A strong correlation was also observed in RNAseq gene expression between feeding arteries and the nidus in surgically acquired bAVMs (Pearson r = 0.95, Figure 3D). This supports that endoluminal sampling from more accessible sites such as juxtanidal feeding arteries is representative of molecular profiles in the AVM nidus without added procedural risk.

Incorporation of CFD Modeling Allows Endoluminal Biopsy to Assay Gene Expression Changes With Alterations in Cerebral Blood Flow

Hemodynamic alterations from cerebral blood flow (CBF) such as wall shear stress are associated with vascular wall remodeling and risk of brain hemorrhage or onset of neurologic symptoms in bAVMs.[27-29] To investigate how CBF alters the transcriptome, CFD modeling from cerebral angiograms was used to compute TAWSS at the site and time of endoluminal biopsy from cerebral angiograms (Figure 4A and Video 2). Across individuals, good correlation between TAWSS and RNAseq gene expression was seen in 11.0% of transcripts (Figure 4B). We identified pathways positively or negatively correlated with TAWSS. This analysis showed enrichment of inflammatory and structural pathways that were negatively correlated with TAWSS (FDR <0.05) (Figure 4C). Ontologic molecular function analyses showed enrichment in binding to RNA and protein kinases and to cytoskeletal elements such as actin and cadherin, consistent with modulatory changes (Figure 4C).

Embolization is an endovascular procedure in which an occlusive material such as a platinum coil or liquid adhesive reduces blood flow and wall shear stress to the bAVM.[30] To confirm our predictions in living patients, we next evaluated the influence of flow-reductive embolization on gene expression in vivo. RNAseq profiling of endoluminal biopsies of the same bAVM arterial segment before and after embolization confirmed differential expression of a minority of

Figure 2 Validation of Endoluminal Biopsy–Detected Brain AVM Gene Expression Changes

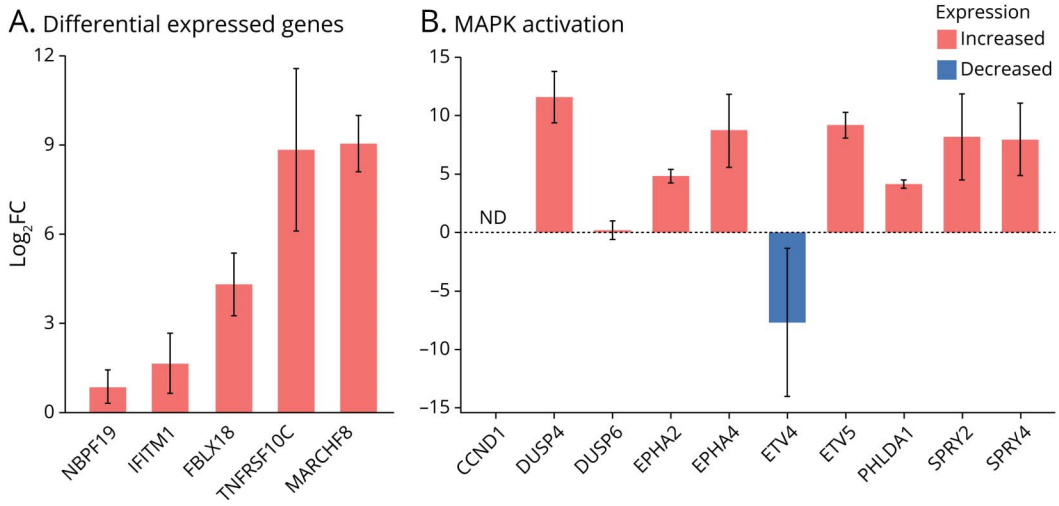

(A and B) Bar graph showing quantitative reverse transcription PCR expression values of differentially expressed genes (A) and gene panel for mitogen-activated protein kinase (MAPK) activation (B). Values expressed as $\log_2$ fold change (Log_2FC) in gene expression in arteriovenous malformation (AVM) vs patient-matched controls. Orange indicates increased expression in AVM; blue, decreased expression in AVM. Data presented as mean ± SEM. ND = not detected.

Figure 3 Endoluminal Biopsy Gene Expression Profiles Show Good Concordance With Open Surgical Sampling

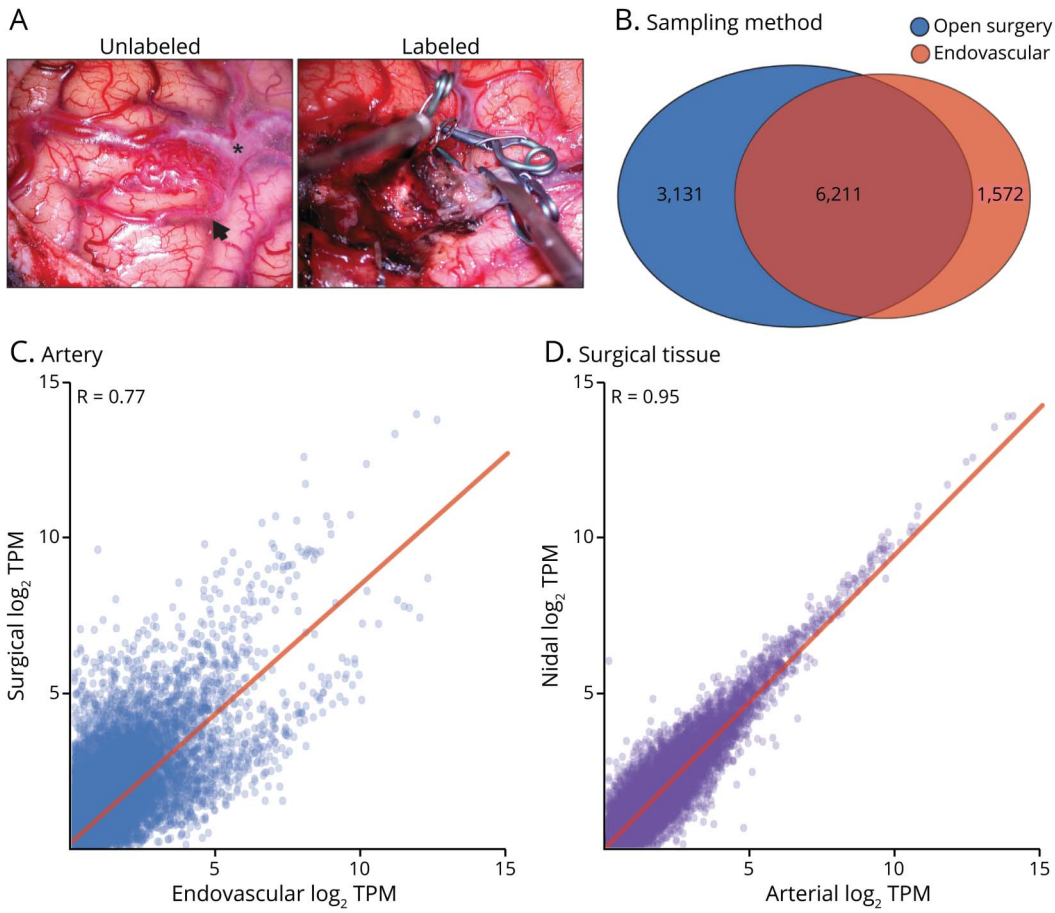

(A) Representative intraoperative microscopy showing microsurgical resection of a brain arteriovenous malformation (AVM). Three-dimensional orientation is preserved with different sizes of aneurysm clips. Arrow shows feeding artery. *Draining vein. (B) Venn diagram comparison of detected genes (transcript per million [TPM] >1) from endoluminal (orange) and open surgical sampling (blue). (C) Scatterplot showing correlation of gene expression from endovascular and surgical sampling from contiguous AVM arterial segment. (D) Scatterplot showing correlation of gene expression of AVM feeding artery and nidus from surgical sampling.

transcripts (7.3%). Consistent with our correlative analyses, genes negatively correlated with shear stress, e.g., expression predicted to increase with lower shear stress, were upregulated in response to flow reduction (Figure 4D). In contrast, genes that correlated positively with shear stress were downregulated in response to reduced flow (Figure 4D). With integration of CFD modeling with gene expression profiling, endoluminal biopsy may facilitate future investigations to understand how alterations in CBF may influence cerebrovascular molecular changes in living patients.

Discussion

Here, we report in-human use of endoluminal biopsy as a means to molecularly profile bAVMs in living patients. We demonstrate that gene expression profiles detect pathogenic and potentially targetable molecular changes in bAVMs without the need for invasive surgery. It is important to note that there is good concordance in gene expression profiling obtained through endovascular biopsy compared to surgically excised tissues (the gold standard). Our results further support involvement of aberrancies in Ras-MAPK signaling in adult bAVMs as previously reported.[5,6] Targeted pathway inhibition such as MEK inhibitors reverses pathologic bAVM endothelial changes in vitro and in vivo and is being trialed in extracranial vascular malformations.[6,7] Our results demonstrate that we are able to detect gene expression alterations that predict response to MEK inhibition in human cancers.[17] Whether this predicts response of human bAVMs to MEK inhibition remains to be determined and is worthy of future investigation.

Incorporation of CFD modeling showed an association of shear stress with gene expression changes and was confirmed by comparing pre-embolization and postembolization gene expression—an intervention modulating shear stress—in human patients in vivo. These analyses support prior in vitro works supporting a modulatory role of shear stress on endothelial inflammatory or cytoskeletal changes.[30-32] Others have suggested that physiologic shear stress is important for other structural elements such as the blood-brain barrier.[33,34]

Figure 4 Flow-Related Shear Stress Influences AVM Gene Expression

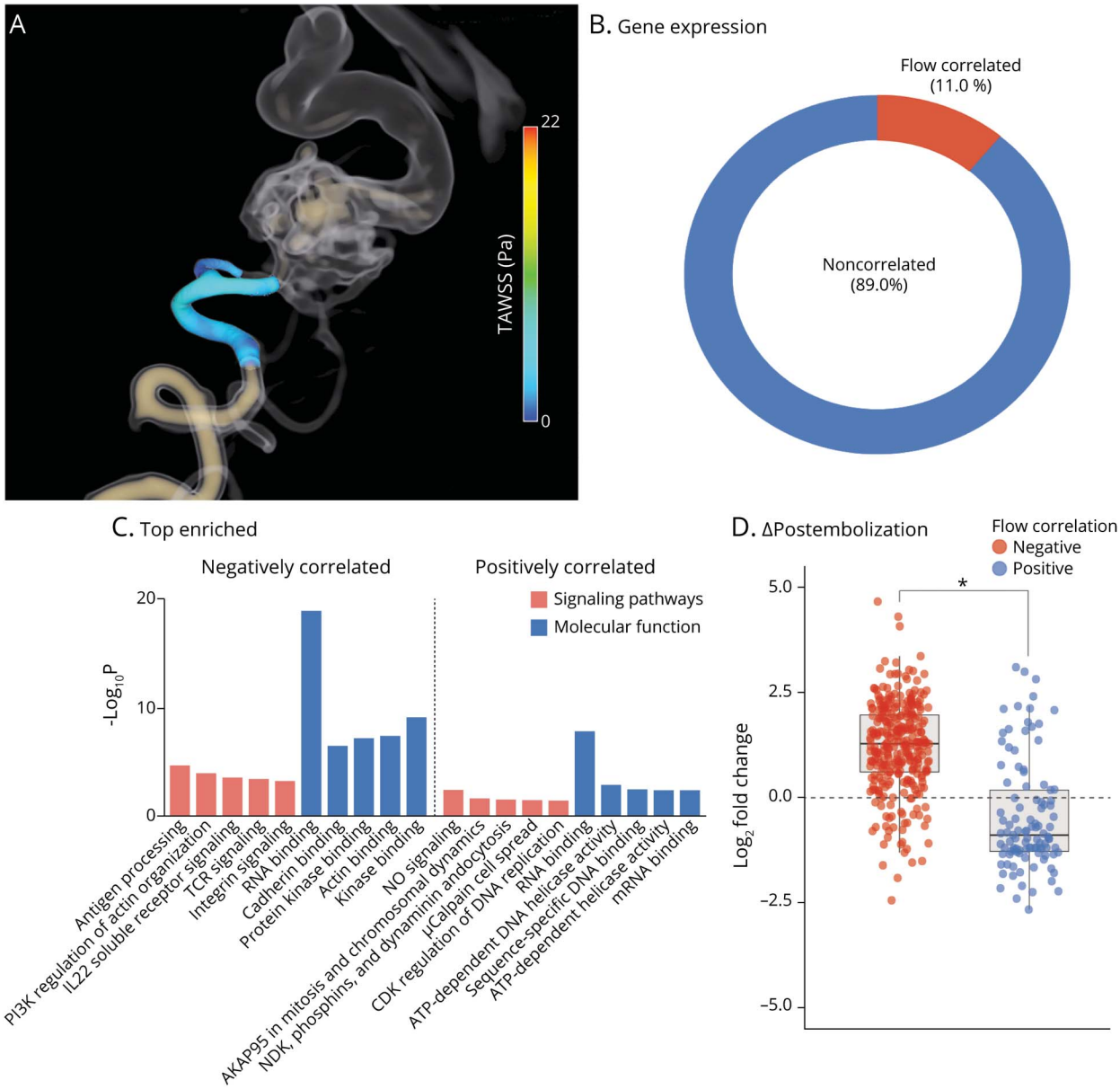

(A) Three-dimensional rotational angiography with computational fluid dynamic shear stress modeling of cerebral angiogram at site of biopsy in arteriovenous malformation (AVM) artery. Injection into vertebral artery. (B) Gene expression. Pie chart showing flow-correlated (orange) and noncorrelated (blue) gene expression. (C) Top enriched. Ontologic analysis of signaling pathways (orange) and molecular function (blue) of flow-correlated genes. Left, negatively correlated; right, positively correlated. Negatively correlated pathways are predicted to be activated with lower shear stress. Positively correlated pathways are predicted to be activated with higher shear stress. (D) Change after embolization. Boxplot of gene expression changes (Δ) after flow-reductive embolization. Orange indicates genes negatively correlated with shear stress; blue, genes positively correlated with shear stress. CDK = cyclin-dependent kinase; IL22 = interleukin-22; NDK = nucleoside-diphosphate kinase; NO = nitric oxide; PI3K = phosphoinositide 3-kinase; TAWSS = time averaged wall shear stress; TCR = T-cell receptor. *$p < 0.05$.

However, our observations were limited to focal segments of feeding arteries at the site of endoluminal biopsy, complicating the interpretation and generalizability of these findings. The hemodynamic environment within bAVMs is immensely complex and currently poorly understood.[35,36] Emerging technologies such as 4-dimensional flow MRI and quantitative magnetic resonance angiography are beginning to shed light on hemodynamic alterations within bAVMs.[27,30,37] Endoluminal biopsies when performed in conjunction with CFD or quantitative MRI may serve as an experimental platform to begin to elucidate the interface between hemodynamic alterations and cellular-molecular changes within bAVMs.

The present study represents a first step in describing application of endoluminal biopsy to molecularly characterize bAVMs in living patients and is not without its limitations, most notably its small sample size and single-center design. All findings should therefore be considered preliminary until further independent

confirmation from other centers to confirm generalizability. Our small sample size demonstrates initial feasibility but is underpowered to determine patient safety. In efforts to validate endoluminal biopsy, comparisons were made with surgically sampled cells from the same patient. Despite minimizing the interval between endoluminal sampling and surgical resection (<24 hours), inflammatory and thrombotic pathways may have contributed to some of the observed differences between endoluminal and surgically sampled cells. Uncertainty surrounding safety with the endoluminal biopsy technique also prohibited collection from uninvolved cerebral arteries. Comparisons were performed between endothelium harvested from bAVM feeding arteries and patient-matched arteries outside the cerebrovasculature near the site of access (e.g., the iliac artery). Transcriptional variation between endothelium between different vascular beds has been reported[38,39] and may have contributed to observed differential gene expression. As safety profiles become better established, future endoluminal biopsy studies should be designed without embolization and should perform comparisons with uninvolved cerebral vessels to confirm these findings.

A pivotal next step is performing larger, multicenter studies to characterize procedure-related safety and complication profiles with endoluminal biopsy. A prevailing safety concern is that endoluminal biopsy would either promote thrombus formation or impair vascular structural integrity, resulting in ischemic or hemorrhagic stroke, respectively. The risk for permanent neurologic complications with diagnostic cerebral angiography due to either ischemic or hemorrhagic stroke is <1%.[40,41] Preclinical testing has shown that deployment of a detachable coil to acquire cells does not lead to angiographic or microscopic damage to the sampled artery.[8] We have also adopted a tiered strategy to mitigate risks of ischemia: (1) systemic heparinization before biopsy, (2) avoidance of flow limitation with coil deployment, (3) limitation of endothelial contact time to 1 minute, and (4) live fluoroscopic monitoring for potential thrombus formation either with coil deployment or immediately after biopsy. With our growing institutional experience, we have yet to encounter a procedural complication associated with endoluminal biopsy applying these strategies. However, the additive risks of performing endoluminal biopsy with a diagnostic cerebral angiogram currently remain unquantified in human patients.

Diagnostic molecular genomics continues to evolve in clinical laboratories, especially within neuro-oncology. Except for the PCR panel predictive of responses to MEK inhibition,[17] the present study uses RNAseq and computational tools that would be difficult to use in larger clinical settings. Ongoing investigations have begun to identify molecular diversity in bAVMs and how it relates to divergent natural histories.[5,6,42] As candidate gene lists become better defined, downstream analytics should use more-targeted gene panels predictive of either therapeutic response or risk for rupture, and we are currently iterating to produce a more targeted test that is not reliant on genome-wide or exome-wide sequencing.

Clinical decisions to treat or monitor vascular malformations are currently informed with imperfect radiologic or clinical surrogates, which may result in divergent natural histories.[43] With further development of endoluminal biopsy, however, it may be possible to directly categorize or serially monitor vascular malformations or other vascular diseases molecularly, much like a tumor. Medical therapy has a favorable safety profile in randomized controlled trials,[3] and endoluminal biopsy could theoretically help identify candidates for targeted precision-based approaches that have shown promise in experimental models.[6,7] Whether endoluminal biopsy will facilitate trials of precision medical therapies in human patients or better identify vascular malformations at greatest risk of bleeding requires further investigation.

Acknowledgment

The authors thank Kenneth Xavier Probst for illustrations in Figure 1.

Study Funding

E.W. is supported by a Brain Vascular Malformation Consortium (BVMC) Pilot Feasibility Project Grant and the Cynthia Lynn Sherwin and Buzz for BAF Chair of Research grant from the Brain Aneurysm Foundation. The BVMC (U54NS065705) is a part of the National Center for Advancing Translational Sciences Rare Diseases Clinical Research Network (RDCRN) and is supported by the RDCRN Data Management and Coordinating Center (U2CTR002818). D.C. is supported through the University of California San Francisco (UCSF) Department of Radiology and Biomedical Imaging, UCSF Research Evaluation and Allocation Committee grant, and Siemens Healthineers AG. K.N. is supported by the BVMC Early Career Enhancement Award (U54NS065705).

Disclosure

The authors report no disclosures relevant to the manuscript. Go to Neurology.org/N for full disclosures.

Publication History

Received by *Neurology* June 3, 2021. Accepted in final form January 11, 2022.

Appendix Authors

Name	Location	Contribution
Ethan Winkler, MD, PhD	Department of Neurological Surgery, University of California San Francisco	Drafting/revision of the manuscript for content, including medical writing for content; major role in the acquisition of data; study concept or design; analysis or interpretation of data
David Wu, BS	Department of Neurological Surgery, University of California San Francisco	Major role in the acquisition of data
Eugene Gil, BS	Department of Neurological Surgery, University of California San Francisco	Major role in the acquisition of data
David McCoy, MS	Department of Radiology and Biomedical Imaging, University of California San Francisco	Analysis or interpretation of data

Continued

Appendix *(continued)*

Name	Location	Contribution
Kazim Narsinh, MD	Department of Radiology and Biomedical Imaging, University of California San Francisco	Drafting/revision of the manuscript for content, including medical writing for content; major role in the acquisition of data
Zhengda Sun, PhD	Department of Radiology and Biomedical Imaging, University of California San Francisco	Major role in the acquisition of data; analysis or interpretation of data
Kerstin Mueller, PhD	Siemens Medical Solutions Inc, Malvern, PA	Analysis or interpretation of data
Jayden Ross, BA	Departments of Neurological Surgery and Anatomy, University of California San Francisco	Major role in the acquisition of data
Helen Kim, PhD	Center for Cerebrovascular Research, University of California San Francisco	Drafting/revision of the manuscript for content, including medical writing for content; study concept or design
Shantel Weinsheimer, PhD	Center for Cerebrovascular Research, University of California San Francisco	Drafting/revision of the manuscript for content, including medical writing for content; study concept or design
Mitchel Berger, MD	Department of Neurological Surgery, University of California San Francisco	Study concept or design
Tomasz Nowakowski, PhD	Department of Anatomy, Department of Psychiatry, Department of Behavioral Sciences, and Eli and Edythe Broad Center for Regeneration Medicine and Stem Cell Research, University of California San Francisco	Drafting/revision of the manuscript for content, including medical writing for content; study concept or design
Daniel Lim, MD, PhD	Department of Neurological and Eli and Edythe Broad Center for Regeneration Medicine and Stem Cell Research, University of California San Francisco	Drafting/revision of the manuscript for content, including medical writing for content; study concept or design
Adib Abla, MD	Department of Neurological Surgery, University of California San Francisco	Drafting/revision of the manuscript for content, including medical writing for content; study concept or design
Daniel Cooke, MD	Department of Radiology and Biomedical Imaging, University of California San Francisco	Drafting/revision of the manuscript for content, including medical writing for content; study concept or design

References

1. Solomon RA, Connolly ES Jr. Arteriovenous malformations of the brain. *N Engl J Med.* 2017;376(19):1859-1866.
2. Lawton MT, Rutledge WC, Kim H, et al. Brain arteriovenous malformations. *Nat Rev Dis Primers.* 2015;1:15008.
3. Mohr JP, Overbey JR, Hartmann A, et al. Medical management with interventional therapy versus medical management alone for unruptured brain arteriovenous malformations (Aruba): final follow-up of a multicentre, non-blinded, randomised controlled trial. *Lancet Neurol.* 2020;19:573-581.
4. Winkler EA, Lu AY, Raygor KP, et al. Defective vascular signaling & prospective therapeutic targets in brain arteriovenous malformations. *Neurochem Int.* 2019;126:126-138.
5. Hong T, Yan Y, Li J, et al. High prevalence of KRAS/BRAF somatic mutations in brain and spinal cord arteriovenous malformations. *Brain.* 2019;142(1):23-34.
6. Nikolaev SI, Vetiska S, Bonilla X, et al. Somatic activating KRAS mutations in arteriovenous malformations of the brain. *N Engl J Med.* 2018;378(3):250-261.
7. Fish JE, Flores Suarez CP, Boudreau E, et al. Somatic gain of KRAS function in the endothelium is sufficient to cause vascular malformations that require MEK but not PI3K signaling. *Circ Res.* 2020;127(6):727-743.
8. Cooke DL, Bauer D, Sun Z, et al. Endovascular biopsy: technical feasibility of novel endothelial cell harvesting devices assessed in a rabbit aneurysm model. *Interv Neuroradiol.* 2015;21(1):120-128.
9. Cooke DL, McCoy DB, Halbach VV, et al. Endovascular biopsy: in vivo cerebral aneurysm endothelial cell sampling and gene expression analysis. *Transl Stroke Res.* 2018;9(1):20-33.
10. Suzuki T, Ioan Nita C, Rapaka S, et al. Verification of a research prototype for hemodynamic analysis of cerebral aneurysms. *Annu Int Conf IEEE Eng Med Biol Soc.* 2016;2016:2921-2924.
11. D'Humières D, Ginzburg I, Krafczyk M, Lallemand P, Luo LS. Multiple-relaxation-time lattice Boltzmann models in three dimensions. *Philos Trans A Math Phys Eng Sci.* 2002;360(1792):437-451.
12. Nita CI, Suzuki T, Itu LM, et al. An automated workflow for hemodynamic computations in cerebral aneurysms. *Comput Math Methods Med.* 2020;2020:5954617.
13. Boegel M, Gehrisch S, Redel T, et al. Patient-individualized boundary conditions for CFD simulations using time-resolved 3D angiography. *Int J Comput Assist Radiol Surg.* 2016;11(6):1061-1069.
14. Karmonik C, Klucznik R, Benndorf G. Blood flow in cerebral aneurysms: comparison of phase contrast magnetic resonance and computational fluid dynamics: preliminary experience. *Rofo.* 2008;180(3):209-215.
15. Foster CH, Morone PJ, Tomlinson SB, Cohen-Gadol AA. Application of indocyanine green during arteriovenous malformation surgery: evidence, techniques, and practical pearls. *Front Surg.* 2019;6:70.
16. Sun Z, Lawson DA, Sinclair E, et al. Endovascular biopsy: strategy for analyzing gene expression profiles of individual endothelial cells obtained from human vessels. *Biotechnol Rep (Amst).* 2015;7:157-165.
17. Wagle MC, Kirouac D, Klijn C, et al. A transcriptional MAPK Pathway Activity Score (MPAS) is a clinically relevant biomarker in multiple cancer types. *NPJ Precis Oncol.* 2018;2(1):7.
18. Fluidigm. D3 assay design. Accessed September 28, 2020. d3.fluidigm.com.
19. Picelli S, Faridani OR, Björklund AK, Winberg G, Sagasser S, Sandberg R. Full-length RNA-seq from single cells using Smart-seq2. *Nat Protoc.* 2014;9(1):171-181.
20. Bray NL, Pimentel H, Melsted P, Pachter L. Near-optimal probabilistic RNA-seq quantification. *Nat Biotechnol.* 2016;34(5):525-527.
21. Stuart T, Butler A, Hoffman P, et al. Comprehensive integration of single-cell data. *Cell.* 2019;177(7):1888.e21.
22. Pimentel H, Bray NL, Puente S, Melsted P, Pachter L. Differential analysis of RNA-seq incorporating quantification uncertainty. *Nat Methods.* 2017;14(7):687-690.
23. Kuleshov MV, Jones MR, Rouillard AD, et al. Enrichr: a comprehensive gene set enrichment analysis web server 2016 update. *Nucleic Acids Res.* 2016;44(W1):W90-W97.
24. Franco CA, Blanc J, Parlakian A, et al. SRF selectively controls tip cell invasive behavior in angiogenesis. *Development.* 2013;140(11):2321-2333.
25. van Nieuw Amerongen GP, Koolwijk P, Versteilen A, van Hinsbergh VW. Involvement of RhoA/Rho kinase signaling in VEGF-induced endothelial cell migration and angiogenesis in vitro. *Arterioscler Thromb Vasc Biol.* 2003;23:211-217.
26. Hauer AJ, Kleinloog R, Giuliani F, et al. RNA-sequencing highlights inflammation and impaired integrity of the vascular wall in brain arteriovenous malformations. *Stroke.* 2020;51(1):268-274.
27. Chang W, Loecher MW, Wu Y, et al. Hemodynamic changes in patients with arteriovenous malformations assessed using high-resolution 3D radial phase-contrast MR angiography. *AJNR Am J Neuroradiol.* 2012;33(8):1565-1572.
28. Chen X, Cooke DL, Saloner D, et al. Higher flow is present in unruptured arteriovenous malformations with silent intralesional microhemorrhages. *Stroke.* 2017;48(10):2881-2884.
29. Winkler EA, Birk H, Burkhardt JK, et al. Reductions in brain pericytes are associated with arteriovenous malformation vascular instability. *J Neurosurg.* 2018;129(6):1464-1474.
30. Alaraj A, Shakur SF, Amin-Hanjani S, et al. Changes in wall shear stress of cerebral arteriovenous malformation feeder arteries after embolization and surgery. *Stroke.* 2015;46(5):1216-1220.
31. DeStefano JG, Xu ZS, Williams AJ, Yimam N, Searson PC. Effect of shear stress on iPSC-derived human brain microvascular endothelial cells (dhBMECs). *Fluids Barriers CNS.* 2017;14(1):20.
32. Inglebert M, Locatelli L, Tsvirkun D, et al. The effect of shear stress reduction on endothelial cells: a microfluidic study of the actin cytoskeleton. *Biomicrofluidics.* 2020;14(2):024115.
33. Garcia-Polite F, Martorell J, Del Rey-Puech P, et al. Pulsatility and high shear stress deteriorate barrier phenotype in brain microvascular endothelium. *J Cereb Blood Flow Metab.* 2017;37:2614-2625.
34. Vatine GD, Barrile R, Workman MJ, et al. Human iPSC-derived blood-brain barrier chips enable disease modeling and personalized medicine applications. *Cell Stem Cell.* 2019;24(6):995.e6.
35. Chang W, Huang M, Chien A. Emerging techniques for evaluation of the hemodynamics of intracranial vascular pathology. *Neuroradiol J.* 2015;28:19-27.
36. Jain MS, Do HM, Massoud TF. Computational Network modeling of intranidal hemodynamic compartmentalization in a theoretical three-dimensional brain arteriovenous malformation. *Front Physiol.* 2019;10:1250.

37. Markl M, Wu C, Hurley MC, et al. Cerebral arteriovenous malformation: complex 3D hemodynamics and 3D blood flow alterations during staged embolization. *J Magn Reson Imaging*. 2013;38(4):946-950.
38. Jambusaria A, Hong Z, Zhang L, et al. Endothelial heterogeneity across distinct vascular beds during homeostasis and inflammation. *Elife*. 2020;9:e51413.
39. Kalucka J, de Rooij LPMH, Goveia J, et al. Single-cell transcriptome atlas of murine endothelial cells. *Cell*. 2020;180(4):764.e20.
40. Dawkins AA, Evans AL, Wattam J, et al. Complications of cerebral angiography: a prospective analysis of 2,924 consecutive procedures. *Neuroradiology*. 2007;49(9):753-759.
41. Willinsky RA, Taylor SM, TerBrugge K, Farb RI, Tomlinson G, Montanera W. Neurologic complications of cerebral angiography: prospective analysis of 2,899 procedures and review of the literature. *Radiology*. 2003;227(2):522-528.
42. Li H, Nam Y, Huo R, et al. De novo germline and somatic variants convergently promote endothelial-to-mesenchymal transition in simplex brain arteriovenous malformation. *Circ Res*. 2021;129(9):825-839.
43. Stapf C, Mast H, Sciacca RR, et al. Predictors of hemorrhage in patients with untreated brain arteriovenous malformation. *Neurology*. 2006;66(9):1350-1355.